

An experimental program for demonstrating precision jet energy measurement at the ILC

Rajendran Raja^{1,*}

¹*Fermi National Accelerator Laboratory,
P. O. Box 500, Batavia, IL 60510*

(Dated: August 8, 2021)

Abstract

We outline a physics program at Fermilab that would significantly improve our ability to understand the behavior of hadronic showers in calorimeters. This would involve a two-pronged approach designed to measure particle production cross sections of hadronic beams on several nuclei to improve shower simulation programs and the validation of the improved shower simulation predictions using test beams (including tagged neutral beams) in which calorimeter modules built using various technologies are deployed in the test beam. Such a program would be of immediate benefit to the efforts to design and build optimal calorimeters for the International Linear Collider.

PACS numbers: 14.20.-c, 14.40.Aq, 14.60.-z

*Electronic address: raja@fnal.gov

I. INTRODUCTION

Hadronic shower simulation programs depend on theoretical models of the strong interaction for generating events that form part of the shower cascade. All these events occur at low enough momentum scales that ensure that they cannot be calculated from first principles using the QCD Lagrangian which is currently only useful in the perturbative regime. The result is that we have a series of event generation models with varying theoretical assumptions that are employed in shower programs that have their own internal parameters which must be tuned to describe particle production data on thin target nuclei to fix their internal parameters.

The data on which the tuning is done are mostly obtained from single particle spectrometers and form a set of varying quality spanning a time period over of thirty years. Most models have sufficient flexibility that their parameters can be adjusted to describe the single variable distributions of the data on which they are tuned.

In ILC calorimeters, both the longitudinal and transverse shapes of showers produced by charged and neutral particles need to be understood. If we can describe the single particle transverse and longitudinal calorimeter energy depositions properly and understand them, we can hope to design the calorimeters that have the appropriate resolution to satisfy the needs of the ILC physics groups.

When we employ models to predict hadronic showers in calorimeters, however, we have to repeatedly generate events and propagate the particles in the media that make up the calorimeter. Correlations (momentum-multiplicity correlations, rapidity correlations, longitudinal-transverse momentum correlations) between individual particles in an event become important as well as the overall inclusive single variable spectra used for tuning the models. The various models will thus diverge in their predictions of showers since the effects of the systematics of the models will be magnified during their repeated use during the showering process.

It is impossible to tune the shower programs using newly acquired calorimeter data, since it is difficult to correlate calorimeter data with the fine structure of the models which generate events at the hadron-nucleus level. What is done currently by some collider experiments is to tune the parameters of the models to test beam data taken on their already designed calorimeters and to use the tuned models as interpolating devices to simulate events in

their full calorimeter. Such tuned models will only work as interpolators in their limited area of tuning but will fail when extrapolated to other materials or momentum regimes or experiments.

The demands of ILC calorimetry are much more stringent than this. One needs to use the models to predict the behavior of showers in calorimetry yet to be designed and then to optimize such calorimetry to obtain hitherto unachieved jet energy resolutions. In order to do this, one needs to improve the status of the simulators by obtaining new multi-particle production data at the particle-nucleus level with excellent statistics, particle identification and acceptance. With such data, the systematics of the models can be controlled to such an extent that the calorimeter shower predictions can be put on a more robust basis.

While this program of improving the shower simulators is going on, we propose to have a program of test beam activity that will test various calorimeter schemes. One needs to decide whether the Particle Flow Algorithm (PFA) [1] is viable or not. This requires the use of tagged neutral beams as well as charged particle test beams using which the behavior of hadronic showers is studied in detail in the calorimeters. The role of compensated calorimetry also should be investigated much more thoroughly, since compensation allows for better linearity and resolution in the calorimeter. Linearity of response is important for both PFA and other algorithms. As we will show subsequently, it may be possible to design calorimeter schemes which provide high resolution spatial information cheaply that can be used for both the PFA as well as compensated calorimetry. We propose that Fermilab embark on a detector R&D scheme to investigate such schemes.

II. IMPROVING HADRONIC SHOWER SIMULATORS

A. Hadronic Production Models and systematics

The current state of hadronic shower simulation programs was examined in great detail at the Hadronic Shower Simulation Workshop [2] held at Fermilab in September 2006. As mentioned, all the simulator programs must rely on models of non-perturbative QCD to make predictions, since we have not yet succeeded in calculating non-perturbative processes from first principles using the QCD lagrangian. These models have free parameters which are tuned to existing data.

In order to illustrate the model dependence, let us consider in some detail the event generator programs DPMJET (Dual Parton Model JET) [3] and QGSM (Quark Gluon String Model) [4]. They both utilize the dual parton model of hadronic production [5] which utilizes the pomeron and reggeon exchanges to describe soft processes. These processes are illustrated in Figure 1. The reggeon exchange diagram can be used to describe a sum of s-channel resonances as well as a sum of t-channel exchanges as these are dual to each other topologically. The pomeron diagram is topologically different from the reggeon exchange planar diagram. When we employ the optical theorem, we can cut the elastic scattering amplitude to reveal the parton structure of the exchange to describe the total cross section. Thus, the reggeon exchange contribution to the total cross section is described by a single quark gluon string whereas the pomeron exchange contribution is described by two such strings.

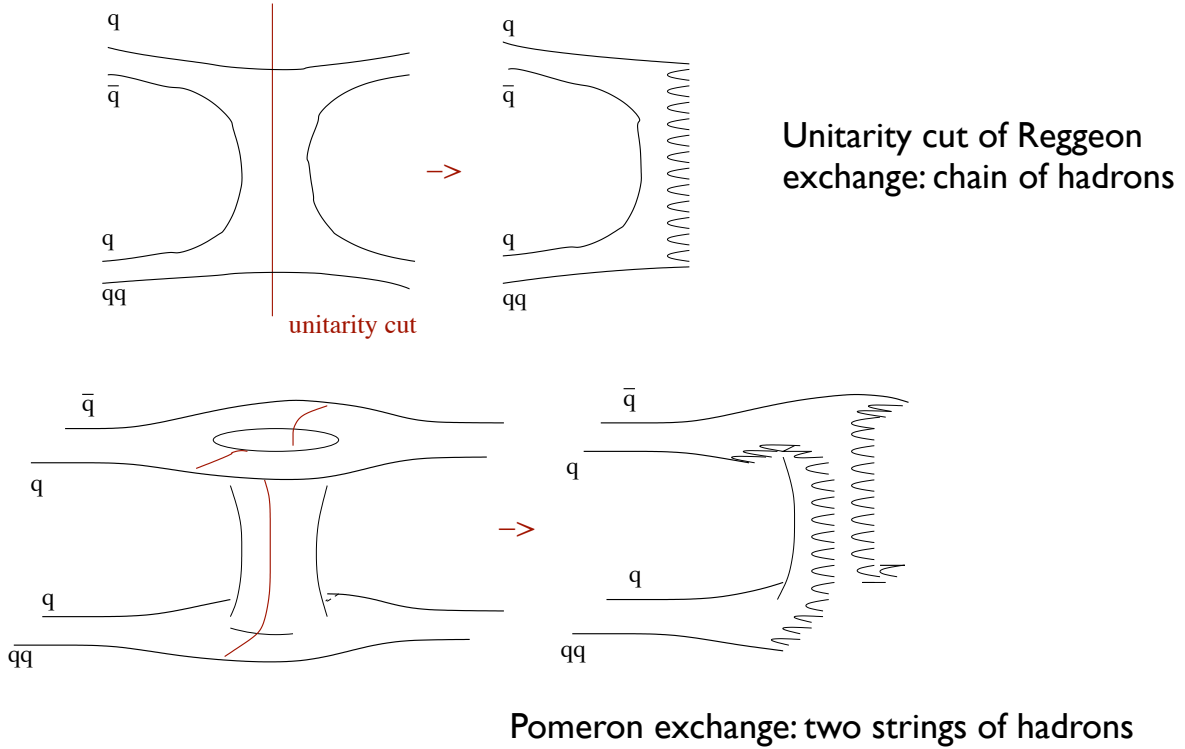
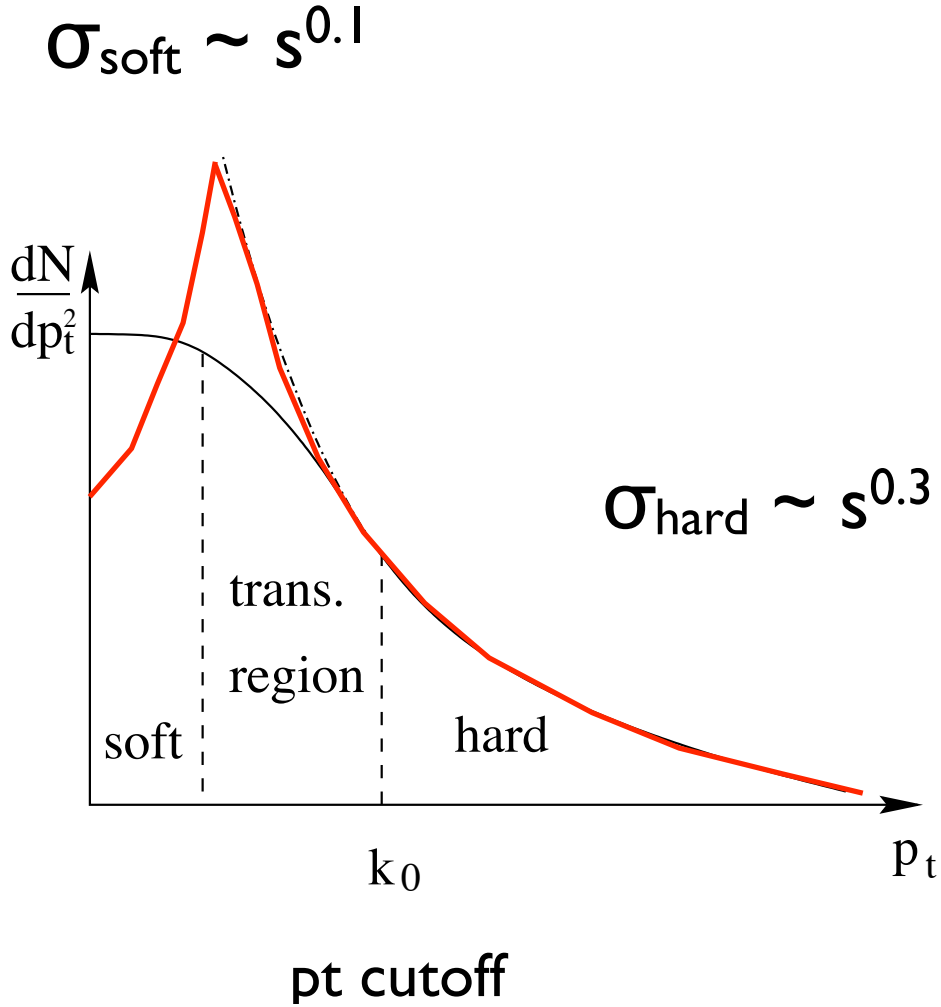


FIG. 1: The topological quark diagram for meson scattering and pomeron scattering. The elastic scattering diagram is cut to produce two strings for a single pomeron exchange. This approach is the basis of the Dual Parton Model employed in DPMJET and QGSM. [6]

At high Q^2 , these strings are described by the (perturbative) parton models and structure

functions, whereas at low Q^2 , the reggeon/pomeron approach is employed. The boundary between these two formalisms is somewhat arbitrary and the joining of the two approaches in itself contains free parameters as illustrated in Figure 2. Finally, none of these models



p_t distribution of partons at string ends

FIG. 2: Matching the energy dependence of the soft processes and the hard processes is done arbitrarily and very carefully [6].

conserve unitarity per se, and unitarity is imposed in DPMJET and QGSM by using the

eikonal approximation. As we go to higher center of mass energy (LHC energies), the number of pomerons exchanged has to be increased to fit the increase in multiplicity. Parton fragmentation into hadrons is an area of considerable uncertainty and is a source of a great deal of systematic differences between the models. Many different hadronization schemes are used each containing a number of tunable parameters. Nuclear fragmentation is also handled differently by different programs. As we will show later, the fragmentation of the nucleus and neutron emission as well as nuclear binding energies have to be simulated well in order to understand the behavior of calorimeters. Table I shows the various simulation programs [7] represented at the Hadronic Shower Simulation Workshop and the models employed by them. It is clear that there is a plethora of models to describe particle production and that none of these models will describe the data perfectly, since there does not currently exist a complete theory of non-perturbative QCD.

TABLE I: Hadronic Shower Simulation Programs represented at the Hadronic Shower Simulation Workshop and the models employed by them.

Program	Event Generator Models	Nuclear Break up models
Fluka05	Isobar model (below few GeV) own version of DPM + hadronization	PEANUT (Includes GINC) Generalized InterNuclear Cascade
Geant4	QGS + Fritiof String model $> 20\text{GeV}$ Bertini Cascade Model $< 10\text{GeV}$ Binary Cascade model Low Energy Parametrized Models & High Energy Parametrized Models (GHEISHA origin)	Geant4 Pre-compound model Bertini evaporation model Chiral Invariant Phase Space model (CHIPS) $< 20\text{MeV}$ Nuclear break-up libraries
MARS15	Inclusive event generator CEM03, LAQGSM03 Quark-Gluon String model	Generalized intra-nuclear cascade evaporation and fission models
PHITS	Jet AA Microscopic Transport Model (JAM) $> 20\text{MeV}$ Jaeri Quantum Molecular Dynamics model JQMD	Neutrons done as in MCNP JQMD
MCNPX	Fluka79 or LAQGSM	Intra Nuclear Cascade models Bertini, ISABEL, CEM, INCL4..

B. The case for obtaining more particle production data

The particle production data on which these models are tuned has been obtained by numerous experiments over the last 30 years. A large number of these experiments are single arm spectrometers and suffer from large systematic errors introduced by the fact a) it is hard to calculate the acceptance of a single arm spectrometer since the acceptance depends on the vertex position (hard to determine if only a single final state particle is measured) and also the cross section one is trying to measure. and b) Corrections due to decay of K_S^0 and Λ particles are hard to make. The cross sections measured by single arm spectrometers are in addition discrete in transverse momentum for the various angular settings of the single arm. Most importantly final particle correlations and multiplicity distributions are not measured.

Figure 3 compares invariant inclusive cross section for two experiments (Allaby et al (1970) [8] and BNL-E941 (2001) [9] for the reaction $p+\text{Be}\rightarrow p+X$ for 19 GeV/c incident protons as a function of the angle of the final state protons. E941 data has to be normalized by a factor 1.6 to agree with Allaby et.al. Figure 4 compares invariant inclusive cross section for the same two experiments for the reaction $p+p\rightarrow p+X$ for 19 GeV/c incident protons as a function of the angle of the final state protons. E941 data has again to be normalized by a factor 1.6 to agree with Allaby et.al. All the models have been tuned to available data and describe the distributions reasonably well. The only proviso is that the distributions are usually functions of one variable only x_F or p_T and do not really attempt to describe the particle correlations. These correlations are of great importance in describe a shower accurately, since a shower with n - generations will magnify the systematic errors n fold. With a view to testing various programs against each other, a set of benchmarks were set before the Hadronic Shower Simulation Workshop [10]. We detail here some of the problem areas.

Figure 5 shows a comparison of the energy deposit as a function of longitudinal depth in a 10 cm Tungsten rod of radius 1 cm as predicted by the programs MARS15, GEANT4, PHITS and MCNPX for 1 GeV/c incident protons. There is significant disagreement between the programs. Figure 6 shows the same plot but with 50 GeV/c incident protons. The discrepancies between the predictions between the various models are still significant.

Figure 7 shows the results of another benchmark test where the program predictions for inclusive proton production are compared to data available for 67 GeV/c incident protons

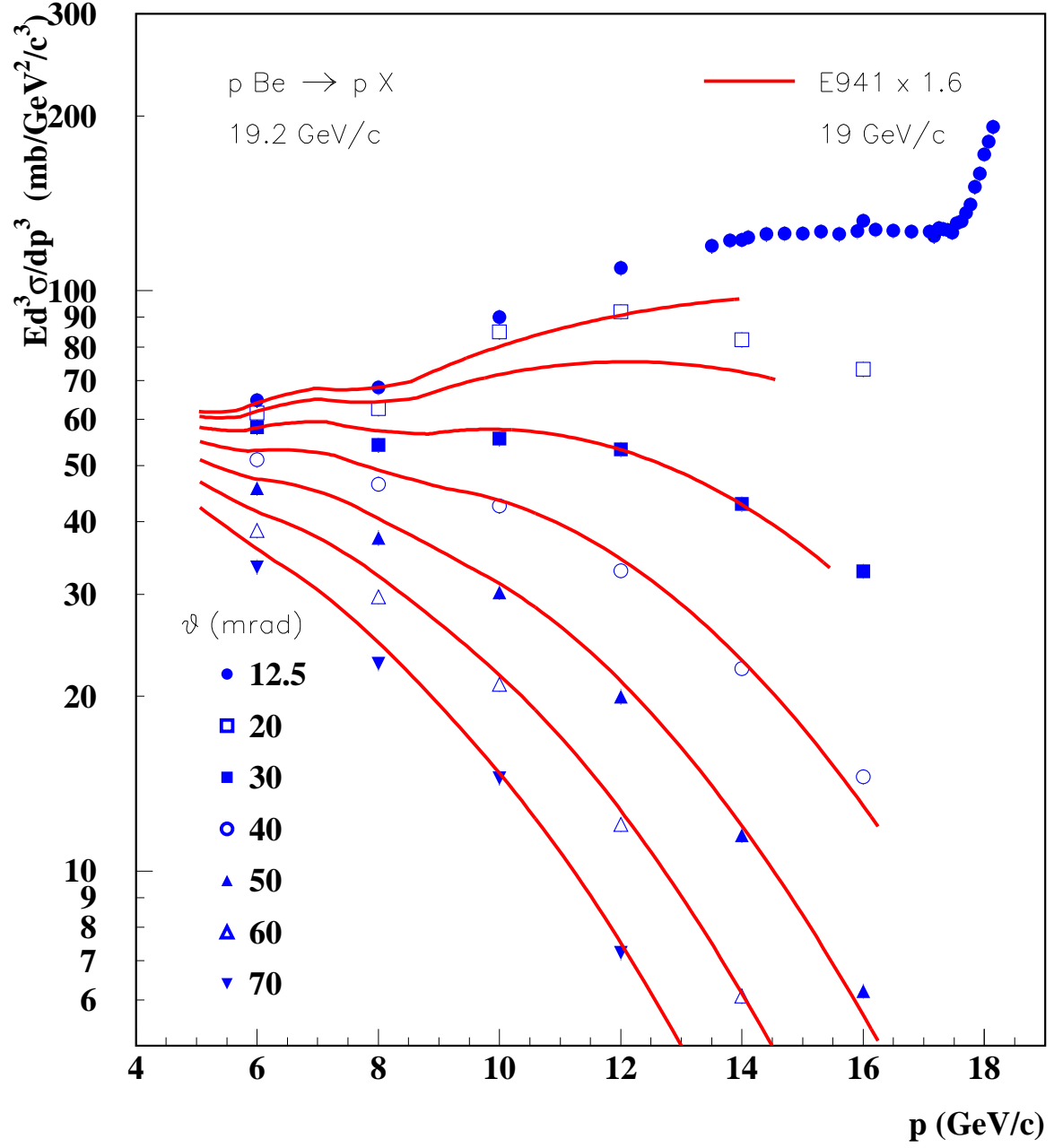


FIG. 3: Comparison of 19 GeV/c proton beryllium data between two different experiments. There is a normalization difference of 1.6 between the two.

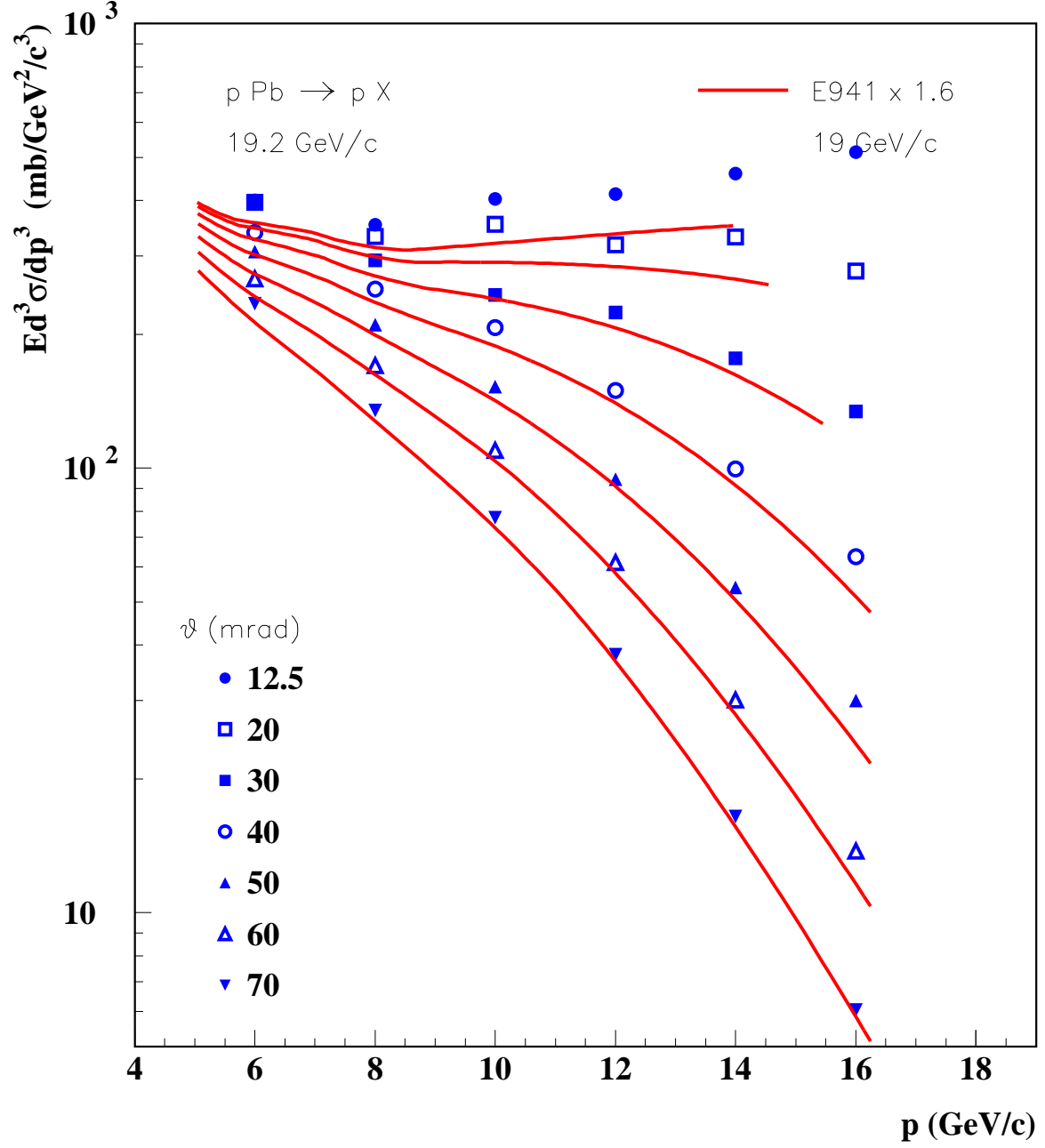


FIG. 4: Comparison of 19 GeV/c proton lead data between two different experiments. There is a normalization difference of 1.6 between the two.

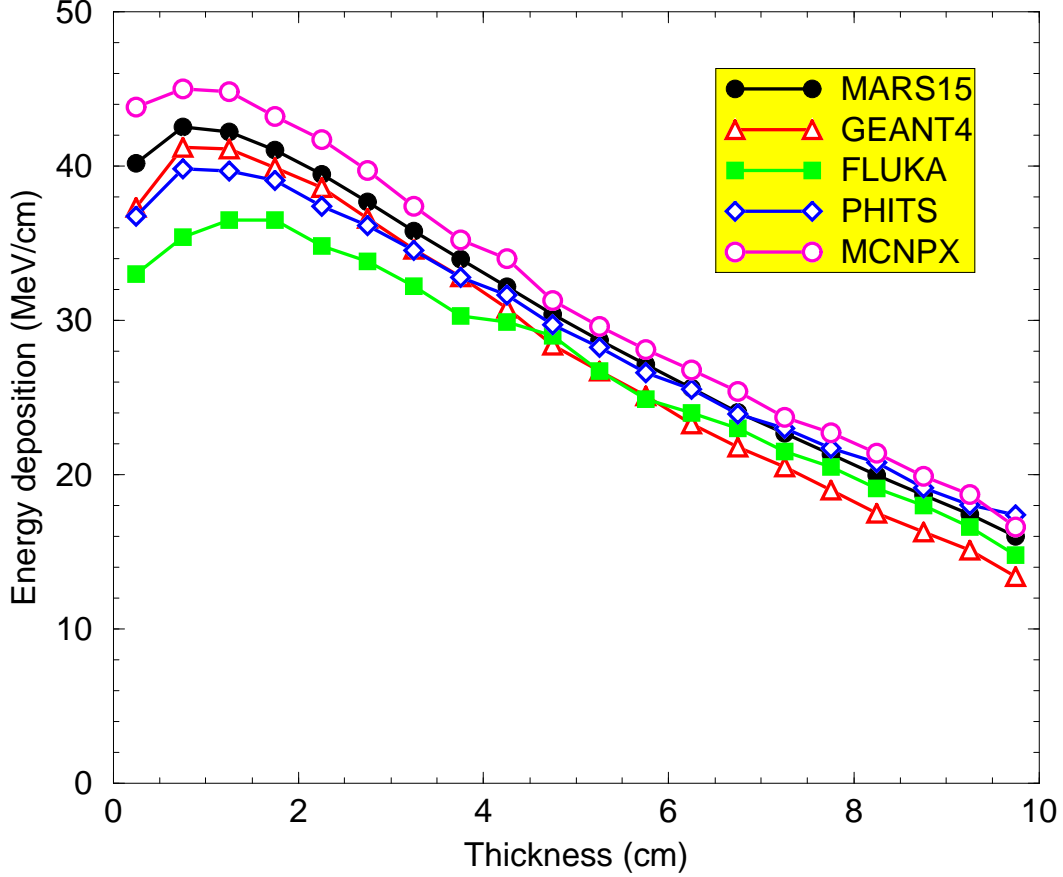


FIG. 5: Energy deposit profile as a function of longitudinal depth of 1 GeV/c protons on a 10 cm Tungsten rod of 1 cm radius. Plotted are comparisons between MARS, GEANT4, PHITS and MCNPX.

on a thick aluminum target. The predictions, plotted as a function of the angle of the final state proton disagree with each other and the data. Similar plots are available for final state pions and kaons with similar degree of discrepancies. We note that this test of the simulators is a crucial benchmark for predicting neutrino spectra for experiments such as MINOS, NOVA and MINERVA. Figure 8 shows the ratio of data/generators (PHITS, MARS and GEANT4) for final state particles π^+ , π^- and p for the angles 5 and 25 mrad as a function of outgoing particle momentum. Discrepancies of the order of a factor of 5 or 6 are evident in some parts of phase space. It must be evident now that ability of the models to predict particle production in conditions where thick targets are used is severely

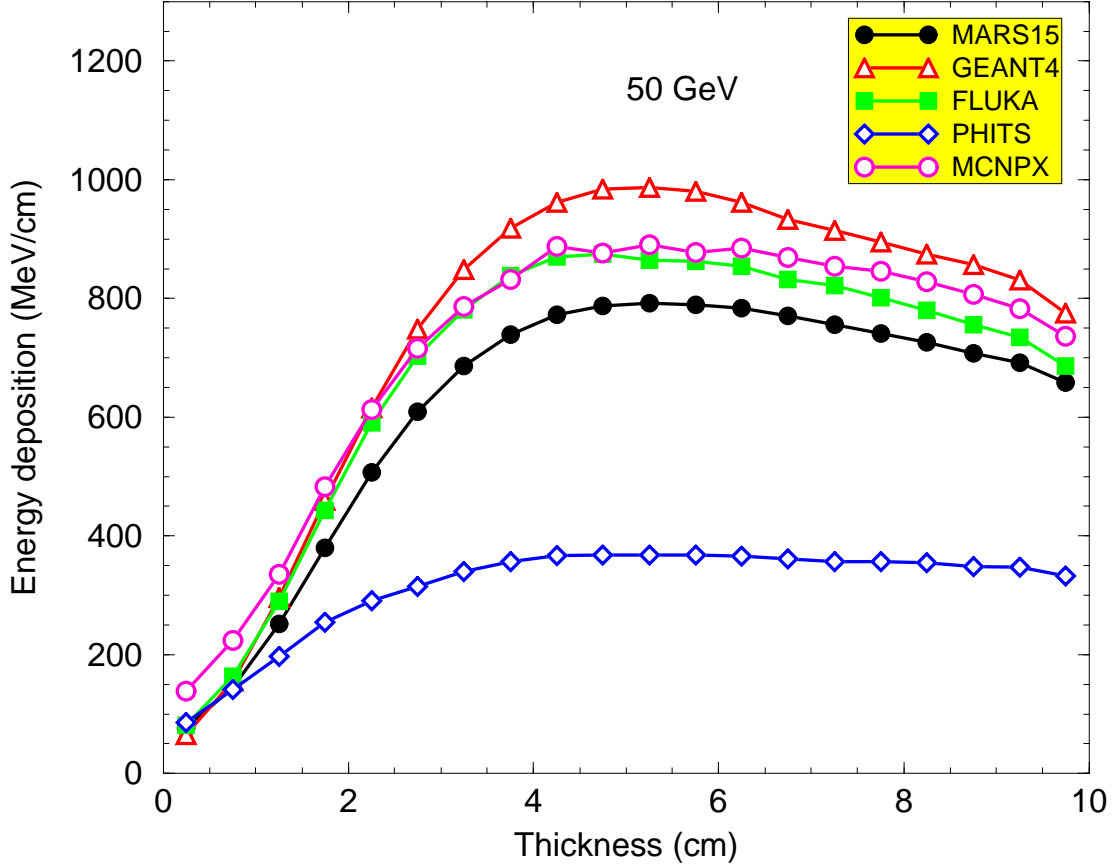


FIG. 6: Energy deposit profile as a function of longitudinal depth of 50 GeV/c protons on a 10 cm Tungsten rod of 1 cm radius. Plotted are comparisons between MARS, GEANT4, PHITS and MCNPX.

under question. It was the unanimous opinion of the simulator experts who participated in the Hadronic Shower Simulator Workshop that high quality multi-particle data with good statistics and particle identification is needed to improve simulators further.

It is not only when the target thickness is changed further that the simulators run into trouble. Similar situation holds when one enters uncharted domains in center of mass energy. Figure 9 shows the prediction of multiplicities and energy distribution of particles in a slice in pseudo-rapidity of $5 < \eta < 7$ at the LHC of various simulators including QGSM, SYBILL and DPMJET. This plot is obtained from the TOTEM experiment at the LHC. there is significant disagreement in the shapes of the distributions between the simulator

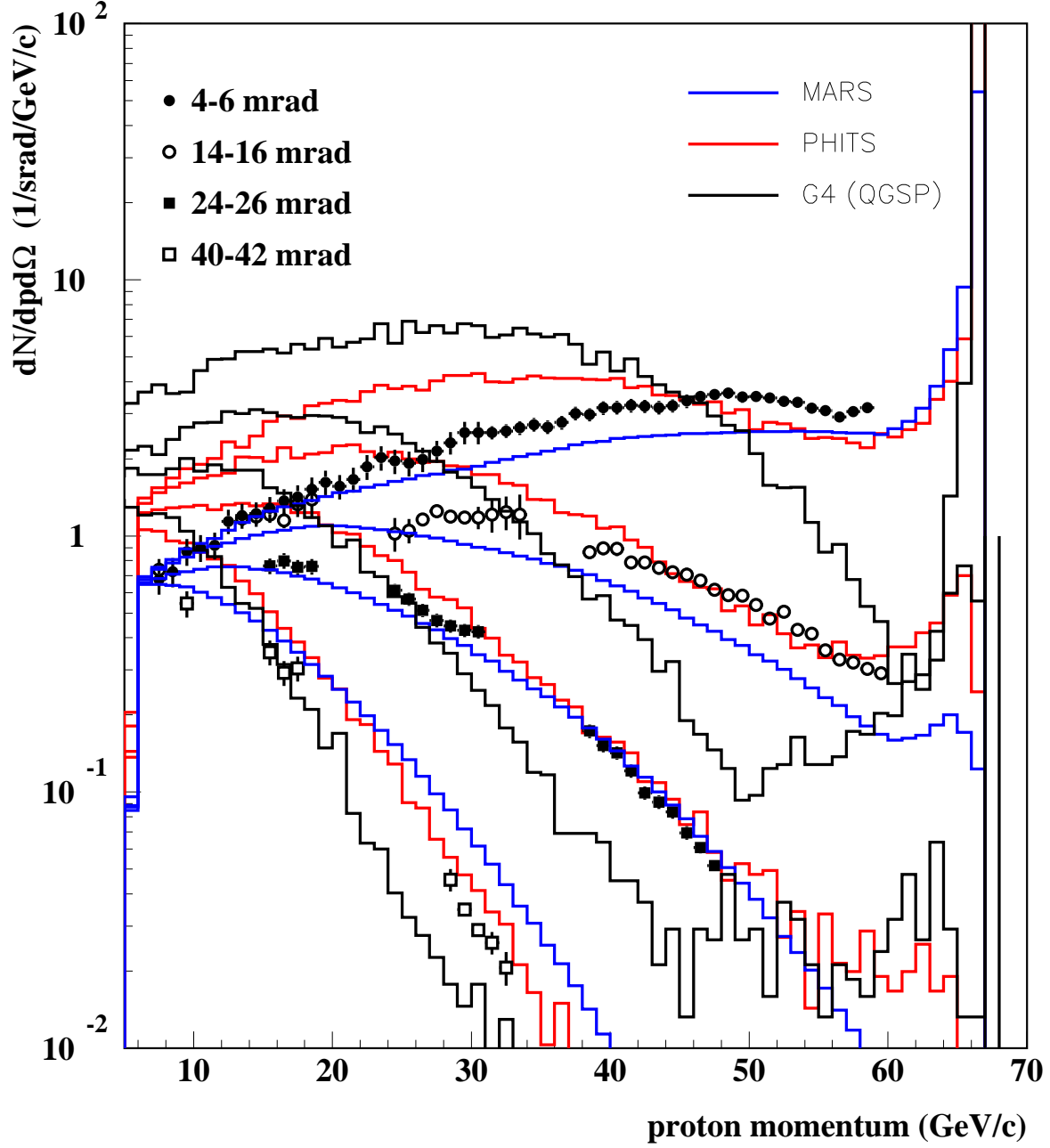


FIG. 7: Comparison of proton production on a thick aluminum target using a beam of 67 GeV/c protons as a function of final state production angle. Plotted are data (symbols) and predictions of MARS, PHITS, and GEANT4 (using generator QGSP) (histograms). There is disagreement between models themselves and models to data.

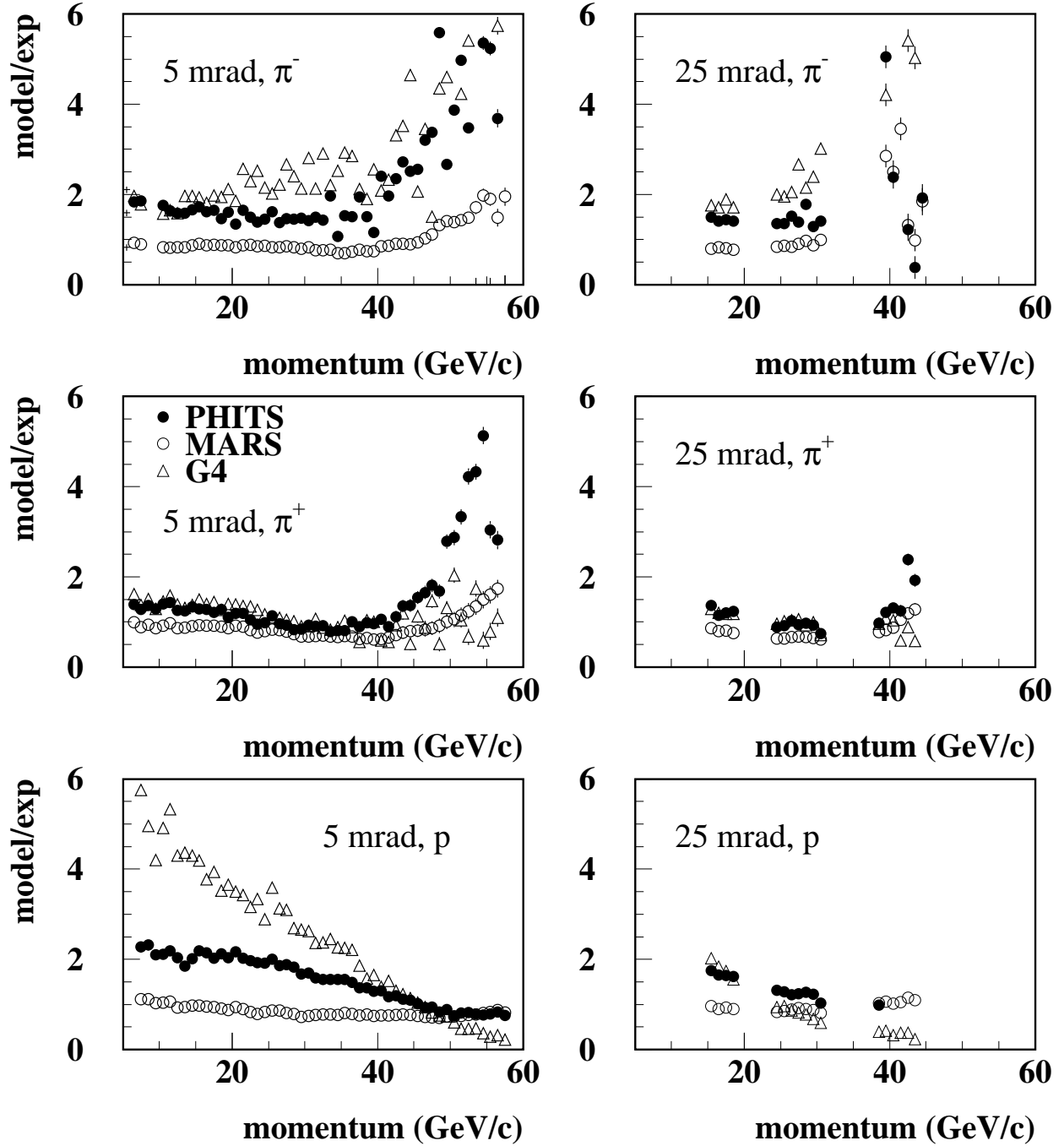


FIG. 8: Comparison of π^\pm and proton production on a thick aluminum target using a beam of 67 GeV/c protons as a function of final state production angle. Plotted are the ratios of predictions of MARS, PHITS, and GEANT4 (using generator QGSP) to data. Open triangles represent Geant4/data, closed circles PHITS/data and open circles MARS/data. Ratios of 5-6 means there is 500-600% disagreement between the specific model and data at that point of phase space!

programs.

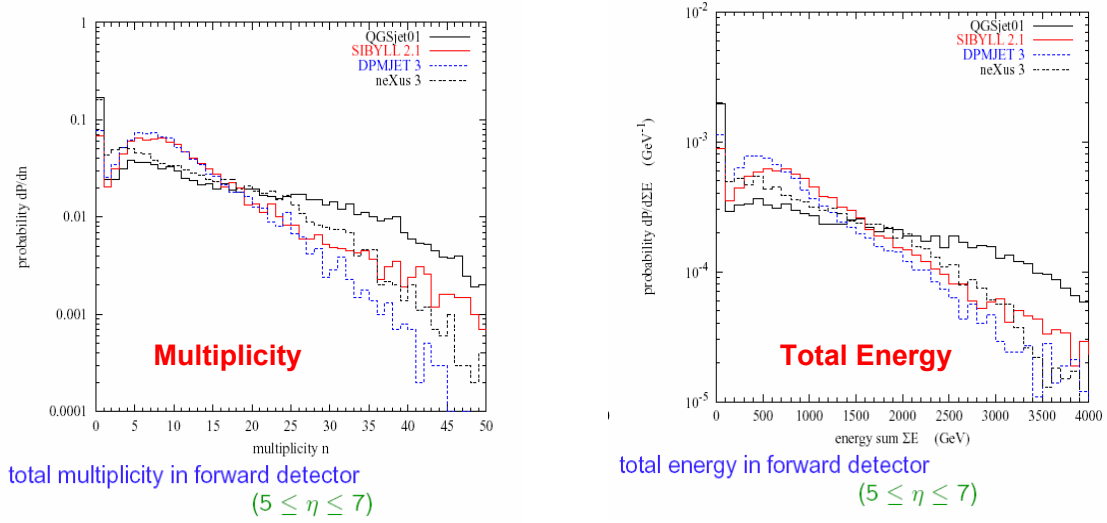


FIG. 9: Comparison of multiplicity and energy distributions in a forward detector at the LHC $5 < \eta < 7$ as predicted by various simulators. Plot courtesy of the TOTEM experiment [11]

C. Possibilities for obtaining high quality data

The MIPP experiment [12] has acquired high quality particle production data on the nuclei H, Be, C, Al, Bi and U with 6 beam species (π^\pm , K^\pm and p^\pm) at various beam momenta ranging from 20 GeV/c to 120 GeV/c. MIPP has acquired 18 million events in total on these targets. MIPP utilizes a TPC which accepts all the particles going forward in the laboratory. Final state particles are identified through all of phase space using a combination of dE/dx , time of flight, multi-cell Cerenkov and RICH technologies. The events are currently being analyzed and papers are expected this year.

The rate of data acquisition in MIPP is limited to 20 Hz by the electronics of the TPC which is 1990's vintage. With more modern electronics, it is possible to upgrade the apparatus to run at 3000 Hz in a cost effective manner. The details of the proposal can be found on the MIPP website [13]. With this increase in speed, it would be possible to acquire 5 million events per day, without any increase in the number of protons being expended by the Main Injector. These numbers are based on a 4 sec-

ond Main Injector spill every 2 minutes with a 42% assumed downtime in beam delivery. MIPP Upgrade proposes to obtain 5 million events per nucleus on the nuclei $H_2, D_2, Li, Be, B, C, N_2, O_2, Mg, Al, Si, P, S, Ar, K, Ca, Fe, Ni, Cu, Zn, Nb, Ag, Sn, W, Pt, Au, Hg, Pb, Bi, U, Na, Ti, V, Cr, Mn, Mo, I, Cd, Cs$ and Ba . Each nucleus requires a single day of running. The data obtained will be put on random access event libraries that are indexed by beam species, beam energy, charged multiplicity and missing neutral mass. These event libraries contain charged particle information and events will contain missing neutrals. The random access library which will fit on 36 Gigabytes of disk can be used directly by the simulation program to look up events close to the particles interacting in a shower. The looked up event can be scaled to the appropriate interacting particle momentum. Missing neutrals can be simulated by using sub-events that have no missing neutrals and converting measured charged particles to neutral particles in a way that conserves isospin. Such an approach will reduce the model dependence of simulation programs and can be rapidly implemented once the DST's are obtained. The feasibility of the random access library scheme can be evaluated even before MIPP upgrade data is available by using the existing simulators to produce simulated thin target data and using this simulated data to populate the library. The test would be to determine how well the library reproduces the simulated data. Such work can be undertaken by people in the simulation groups. Expertise in random access databases would be very valuable here.

A parallel approach will be to fit the models to the new data, but since there is no exact theory, there are no exact models and it may be difficult to fit all this data with a single set of model parameters.

It should be pointed out that improving hadronic shower simulators will benefit a broader community than the ILC effort. The neutrino program, the collider programs, cosmic ray air showers and atmospheric neutrino communities have systematics associated with shower simulations that need to be brought under better control.

III. CALORIMETER RESOLUTION

The resolution of hadronic calorimeters has been extensively studied [14] and the effects of unequal responses to hadronic and electromagnetic energy has been extensively reported. A pion of 1 GeV energy interacting in lead on average deposits only 0.478 GeV as ionization and

loses 0.414 GeV as binding energy involved in nuclear break-up, 0.126 GeV into evaporation neutrons and 0.032 GeV into target recoil energy. Electromagnetic showers deposit all their energy as ionization. This leads to an e/h ratio that is significantly larger than unity unless steps are taken to compensate for the missing energy in hadronic reactions. This imbalance in response is the source of two problems in hadron calorimetry namely a degradation in energy resolution and non-linearity of response. The degradation in energy resolution is the result of fluctuations in the EM/Hadron energy from shower to shower due to the random nature of the showering process.

While reconstructing the shower, under the assumption that one cannot tell apart the EM energy from the hadronic energy, one is forced to use a single set of calibration constants for each shower which results in a degradation of energy resolution.

A. Constant term in resolution due to non-compensation

The unequal response to electromagnetic and hadronic energies results in a constant term in the resolution function as can be seen trivially by

$$E_{vis} = E_{em} + fE_{had} \quad (1)$$

E_{vis} is the energy deposited as dE/dx in a single hadron shower in the calorimeter, E_{em} is the energy deposited as electromagnetic energy in the shower and E_{had} is the energy deposited as hadronic energy in the shower, and f is the e/h ratio. Let E_{live} be the energy observed in the live sampling layers of the calorimeter. Then

$$E_{live} = E_{vis}/\mu \quad (2)$$

where μ is the inverse sampling fraction of the calorimeter. Let E_{true} be the true energy of the parent hadron and let λ be the fraction of the energy in hadronic energy and $1 - \lambda$ be the fraction in EM energy. λ fluctuates from event to event. Then one can write for a single event

$$E_{live} = E_{vis}/\mu = \frac{(1 - \lambda)E_{true} + f\lambda E_{true}}{\mu} \quad (3)$$

This can be re-written

$$E_{live} = \frac{((1 - \lambda(1 - f))E_{true}}{\mu} \quad (4)$$

E_{true}/μ can be thought of as the ideal energy observable in a calorimeter with $e/\pi = 1.0$. This then yields

$$E_{live} = ((1 - \lambda(1 - f))E_{live}^{ideal}) \quad (5)$$

Taking logarithms and differentiating to calculate variances, one gets,

$$\frac{\sigma_{E_{live}}}{E_{live}} = \frac{\sigma_{E_{ideal}}}{E_{ideal}} \oplus \sigma_{\lambda} < \frac{(1 - f)}{1 - \lambda(1 - f)} > \quad (6)$$

The term $\frac{\sigma_{E_{ideal}}}{E_{ideal}}$ will scale as $1/\sqrt{(E)}$ where as the term $\sigma_{\lambda} < \frac{(1-f)}{1-\lambda(1-f)} >$ will act as a constant term that vanishes in a perfectly compensating calorimeter with $f = 1$. The brackets $<>$ denote r.m.s over events, and the symbol \oplus denotes addition in quadrature. For high energies, the constant term dominates the resolution and should be made as small as possible while designing the calorimeter.

B. Non-linearity in energy response due to non-compensation

The non-linearity results from the fact that the fraction of EM energy that hadronic showers deposit increases with the energy of the parent hadron, because EM showers do not produce further hadrons where as hadrons can continue to give more EM energy further in the cascade.

The effect of calorimeter non-compensation can be seen in the CMS detector, where two different technologies (crystals for EMCAL + steel/scintillator for HCAL) produce significant lack of compensation and non-linearities in the calorimeter hadronic response. Figure 10 shows the significant non-linearity to test beam pions with both EMCAL and HCAL and Figure 11 shows the much better response of the hadronic calorimeter by itself. Unfortunately while taking data, both EMCAL and HCAL come into play for hadrons and non-linearities will effect jet and missing E_T reconstruction. For the ILC, even if we succeed with the PFA algorithm, a non-compensated calorimeter will make the response to the neutral hadrons detected in the HCAL non-linear.

Calorimeter compensation can be achieved by two different techniques- The first is by making the neutrons interact with hydrogenous material that result in highly ionizing energy deposit from knock-on protons. The fraction of hydrogenous material is carefully tuned to achieve the right amount of boost in the hadronic response to compensate for the energy lost in nuclear break-up. This approach was used in the DØ calorimeter and the Zeus calorimeter

both of which had e/π ratio close to unity. A single particle resolution of $30\%/\sqrt{(E)}$ was achieved in the the Zeus calorimeter.

The other approach for compensation is to obtain separate signals from the electromagnetic energy and the hadronic energy (using fibers sensitive to Cerenkov and scintillator light) and weight these two separately to optimize the resolution. This is the approach taken by the DREAM calorimeter, the 4th concept of the ILC detector. We emphasize

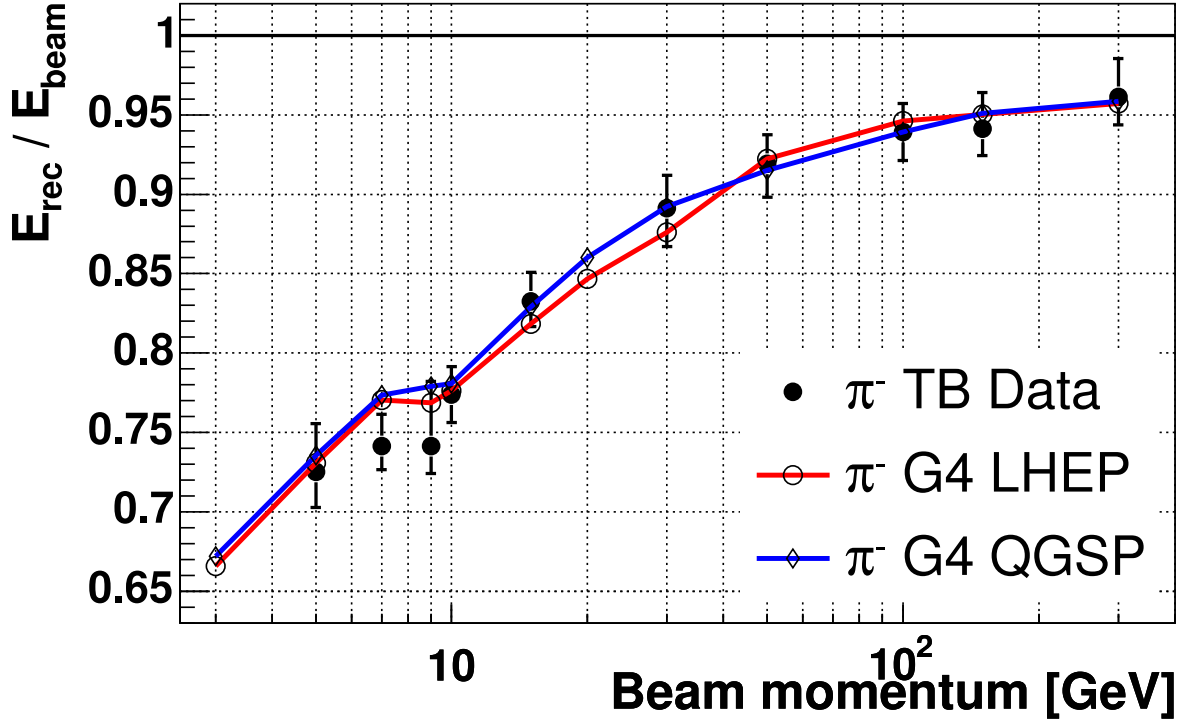


FIG. 10: CMS linearity plot with EMCAL and HCAL [15]

here that it is possible to have both a compensated calorimeter and employ the PFA algorithm, if sufficient care is taken to design and build such a calorimeter. Before we propose a scheme that will serve both purposes, we point out the need for longitudinal segmentation in a sampling calorimeter.

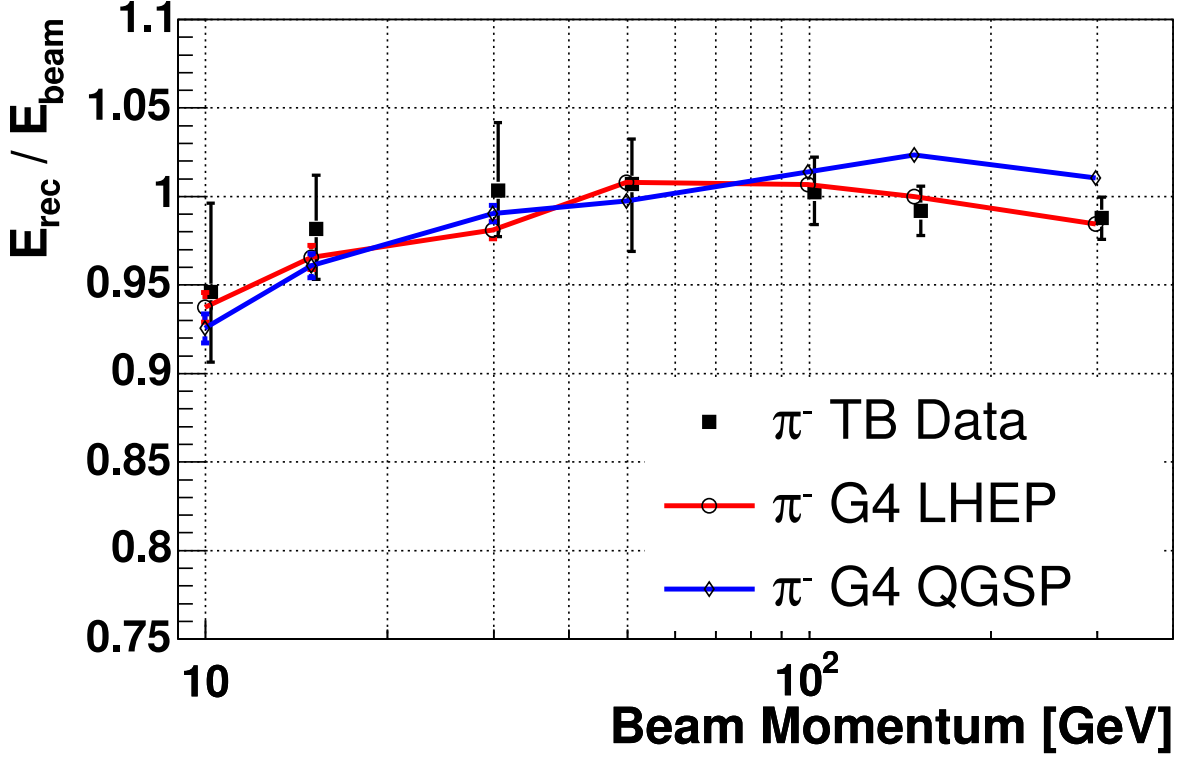


FIG. 11: CMS linearity plot with HCAL only [15]

C. The case for longitudinal segmentation

There exist two different methods for calibrating sampling calorimeters. One is to multiply the live energy in each layer by the inverse sampling fraction yielding

$$E^{\text{deposited}} = \sum_{i=1}^{i=N_{\text{layers}}} \mu_i E_i^{\text{live}} \quad (7)$$

This will give you the total energy on average but the resolution will **not** be optimal as has been shown in [16]. This is a result of correlations between layers (longitudinal and transverse) in a shower.

It can be shown that the best estimator of energy deposited in a layer, that optimizes resolution [16] is given by

$$E_i^{\text{deposited}} = \sum_{j=1}^{j=N_{\text{layers}}} \lambda_{ij} E_j^{\text{live}} \quad (8)$$

where the matrix λ_{ij} (also referred to as the λ tensor) is in general non-diagonal.

Then the best estimate of the deposited energy is

$$E_{deposited} = \sum_{j=1}^{j=N_{layers}} w_j E_j^{live} \quad (9)$$

where the weights w_i are in general not equal to the inverse sampling fractions and are given by

$$w_j = \sum_{i=1}^{i=N_{layers}} \lambda_{ij} \quad (10)$$

Figure 12 shows the reconstructed energy of 100 GeV electrons using the inverse sampling fraction method and Figure 13 shows the same data reconstructed using the weights method [16]. It can be seen that the weights method gives superior resolution. The formalism developed in [16] was for EM showers, but applies equally to hadronic showers. In fact, it can be shown that the inverse sampling fraction method and the weights method become identical only in calorimeters where the sampling fraction is unity and the λ matrix is diagonal. In all other cases, the weights method will give better resolution.

The λ tensor can only be worked out if Monte Carlo information is available. However, the weights w_i , which are used for calibrating the calorimeter in practice can be derived from test beam data using linear least squares minimization to optimize the resolution. The weights, being the sum of the rows of the λ tensor, are essentially non-local in nature and involve properties of the entire calorimeter. They give better resolution by taking into account shower correlations. The DREAM [17] calorimeter using fibers to read out EM and hadronic showers will give superior resolution. It is however difficult to segment longitudinally.

The case for longitudinal segmentation can be enhanced on pattern recognition grounds as well.

D. A possible way to achieve a highly segmented compensating calorimeter cheaply

We now illustrate the possibilities of using a liquid argon TPC with absorbers as a calorimeter. The whole physics case is predicated on the premise that the event rate at the ILC is low enough that event readout times of the order of a millisecond are tolerable.

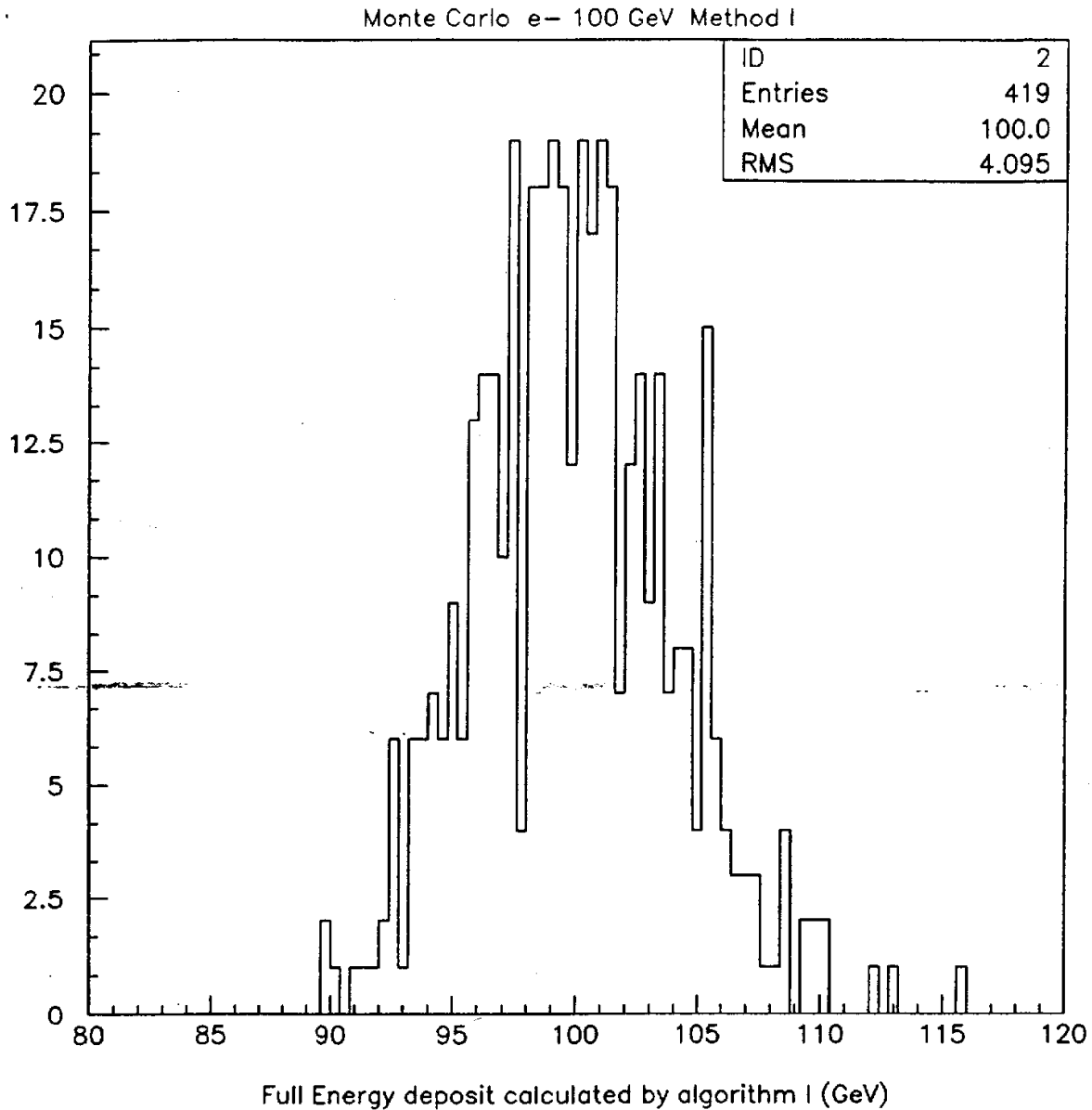


FIG. 12: Reconstructed energy of 100 GeV electrons using the inverse sampling fraction method [16]

If this is the case, the following scheme can be used to produce cheap, highly segmented compensating calorimeters that will also serve the purposes of the PFA algorithm.

Figure 14 illustrates the scheme. Absorber plates of thickness $\approx 3\text{mm}$ are immersed in liquid argon. The liquid argon gap is also $\approx 3\text{mm}$. It is probably best if the absorber material is insulating. In each liquid argon gap, we construct a field cage using copper strips engraved on a thin insulating sheet of material attached to the absorber. This field cage

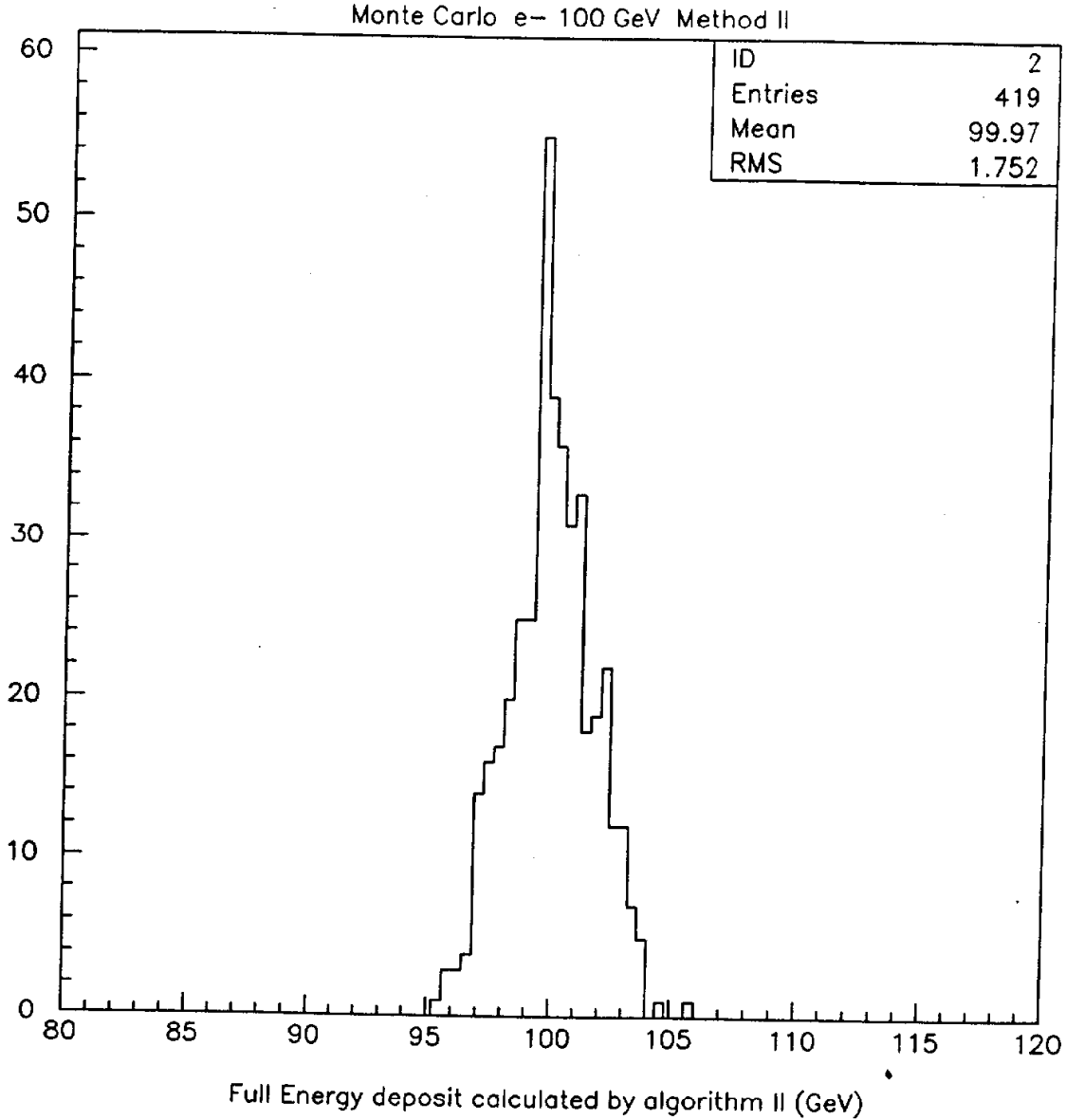


FIG. 13: Reconstructed energy of 100 GeV electrons using the weights method [16]

will then support electric fields in the argon of 500 V/cm. The drift velocity in argon is 1.5meters/millisecond. So if one is allowed a drift time of 0.5 millisecond, one can construct calorimeter modules of 75 cm long in the drift direction. The drifted charge is then measured by the standard technique of a gating grid and anode wires and pads. The longitudinal segmentation is governed by the size of the pads. In the transverse direction, the time measurement will yield TPC like resolution of the shower.

The diffusion of charge in liquid argon is ≈ 1.3 mm σ after a drift time [18] of 3 mil-

lisecond. This means that a liquid argon gap size of 3 mm is sustainable for a drift time of 0.5 millisecond.

$E \times B$ effects in the drift will cause some distortion of the track positions in the calorimeter as a function of drift time. In the barrel region, the drift is along the solenoidal magnetic field, so these effects are negligible. In the end-cap region, one can still continue to drift along the field direction or better still one can calibrate away the $E \times B$ effects.

The readout area has to be made as thin as possible, since it cannot sustain absorbers and thus represents a crack. The effects on hermeticity of these cracks can be ameliorated by staggering adjacent modules to avoid pointing cracks.

The liquid argon cryostat is another area where hermeticity may be an issue. This can be considerably ameliorated by using aluminum to construct the cryostat and by using “absorber gaps” to read out the shower immediately after the cryostat. Since the first piece of material (ignoring the tracker) seen by the hadrons is the cryostat, its effects on resolution are substantially reduced.

Compensation in such a device is attained by “pattern recognizing” (either online or offline) the electromagnetic showers by the local density of tracks associated with them and separating them from hadronic tracks this way. This then permits one to use two sets of weights for EM and hadronic deposits leading to compensation. One can fine tune the hydrogenous content in the calorimeter to tune out the fluctuations in nuclear break up to obtain even better resolution.

Such a calorimeter, if realized, is cheap, highly segmented longitudinally and transversely, compensating and suitable to be used with the PFA algorithm.

We note that such a device would also serve as a far detector for a neutrino factory since it can be made compact enough to sustain magnetic fields affordably and the oscillation $\nu_e \rightarrow \nu_\mu$ in the neutrino factory is detected by the appearance of wrong sign muons. By reducing the absorber thickness and using appropriate absorber materials, one may even be able to use this device to search for rare decays of nuclei in the absorber.

The device proposed here will be comparatively inexpensive to build for a given segmentation than other technologies, since the time (drift) dimension is as long as 75 cm and does not need to be instrumented to obtain the segmentation.

The ILC detector concepts currently under consideration [19] consist of the GLD, LDC, and SiD detectors with the DREAM calorimeter forming the center point of the 4th detector

Liquid Argon TPC Calorimeter Schematic

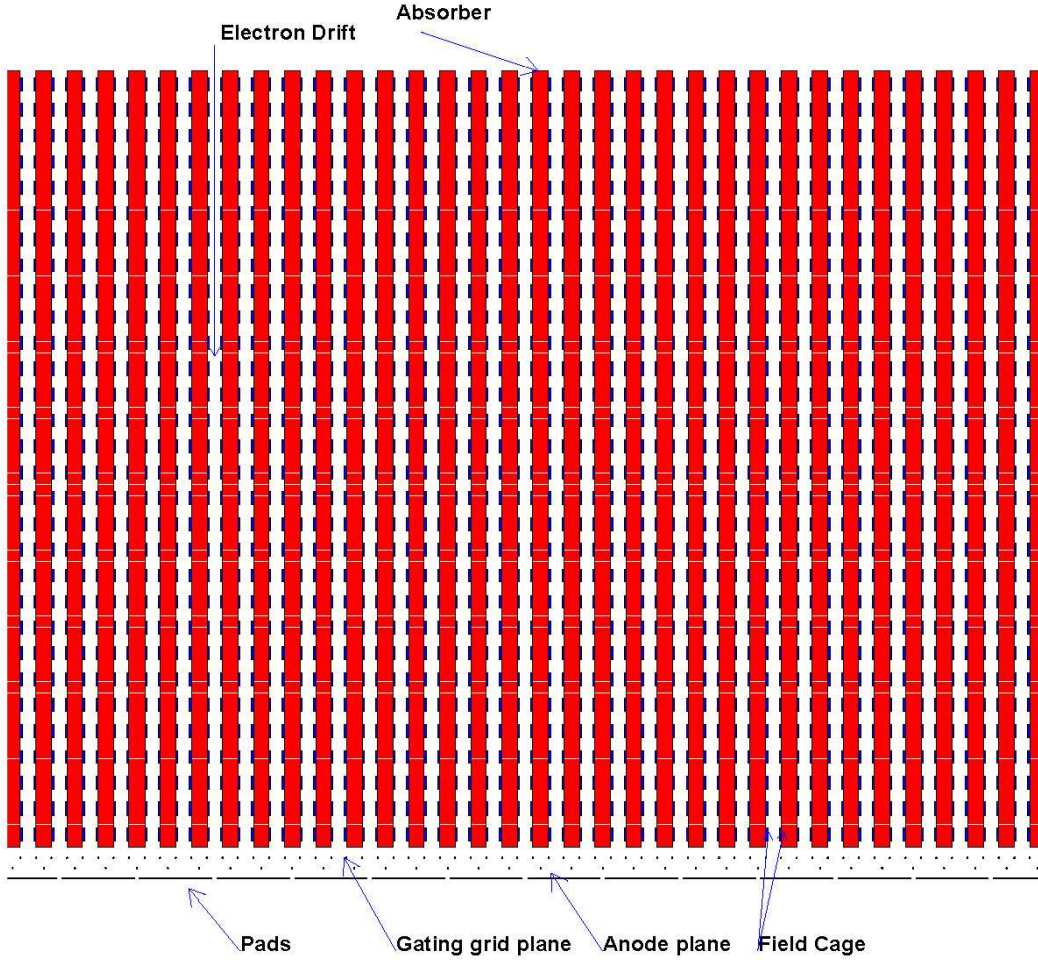


FIG. 14: Schematic of a liquid argon TPC calorimeter with absorber, field cage, gating grid, anodes and pad shown. Beam enters left to right, and electrons drift downwards. The absorber and liquid argon gaps are comparable in size. The drift field is maintained in the gap by means of a field cage in each gap. The longitudinal segmentation is governed by the size of the pads and the transverse segmentation is provided by the drift time measurement. Compensation is achieved by being able to distinguish EM deposits and hadron deposits by the track density.

concept. The GLD concept uses Tungsten (W)/Scintillator for its EM calorimeter, Pb/Scint for the HCAL, and W/silicon and W/Diamond technologies for its forward calorimeters. The LDC design has an EM calorimeter that uses Silicon-Tungsten and a hadronic calorimeter made of iron/scintillator. The SiD detector also employs Silicon-Tungsten for the EM

calorimeter and is doing R&D on the hadronic calorimeter readout to choose between GEM's, Scintillator, RPC's and silicon PMT's. All the detector groups except the 4th concept employ the PFA algorithm to obtain good resolution and the calorimetric designs are driven towards high segmentation (and expense) based on the needs of the PFA algorithm.

E. Test beam activity

The calorimeter modules being constructed using various technologies should be tested in charged particle beams that range in momentum from $\approx 1 \text{ GeV}/c$ to $100 \text{ GeV}/c$. One needs to test the calorimeter response to both positive and negative beams with identified beam particles π^\pm, K^\pm, p^\pm .

Such beams are available at CERN and at Fermilab M-Test area, where a new beamline has recently been commissioned (shortened and upgraded, using experience gained in the MIPP beamline design) to provide lower energy beams.

Such an activity can help debug the electronics and test the design of the modules by comparing the test beam response (longitudinal and transverse) to hadronic shower simulation programs. It is unlikely that one hadronic shower simulation program out of the many available can be used to fit all the data over all momentum and beam species for all the technologies. One approach to take then would be tune the parameters available in some of the models to a chosen technology. But such a tuned model, if it works adequately will only work for that technology and likely not for others. As mentioned previously, improving shower simulation programs needs data at the hadron nucleus level using a particle production experiment. The direct usage of events in simulation programs from random access libraries will help reduce the model dependence considerably.

There is much less particle production data that have neutrons, K_L^0 and anti-neutrons as beams compared to charged particle production data. The neutral particle response in calorimeters is also thus harder to predict well. The PFA algorithm proposes to measure the charged particle energies using magnetic fields and to use the calorimeter for neutral particle energy measurements (EM and hadronic). In order to separate the neutral and charged hadronic deposits in the calorimeter in a jet, it is thus necessary to understand the transverse and longitudinal deposition characteristics of both the charged and neutral particles.

It is here that the tagged neutral beam capabilities of an upgraded MIPP experiment can help the ILC effort.

F. Tagged Neutral beams and ILC Detector R&D

Three out of the four ILC detector concepts (SiD, LDC, GLD) [19] are optimized around the particle flow algorithm (PFA), which proposes to measure the energy of jets in an event by using both the magnetic field and the calorimeter. The charged particles are measured using the excellent momentum resolution of the tracker and the neutral particles are measured using the calorimeter. The required fractional energy resolution of a jet is $\sigma_E/E = 0.3/\sqrt{E}$, E in GeV. This hard-to-achieve performance is driven by the ILC design requirement to be able to separate the processes $W \rightarrow jet + jet$ and $Z \rightarrow jet + jet$. In order to measure the neutral particle energy using the calorimeter, one needs to separate the charged particle hits and the neutral particle hits in the calorimeter. This dictates a highly segmented calorimeter. In order to test the design, one needs to simulate the widths of the showers of both the charged and neutral particles in the calorimeter. Figure 15 shows the simulation of the width a 10 GeV π^- particle entering two ILC calorimeters, one using RPC readout and the other using scintillator readout [20] for a variety of hadronic shower simulators available in Geant4 and Geant3. The widths are normalized to the narrowest width obtained. There is a variation in the widths of 40% in the simulations. This calls for a data-based approach both for charged and neutral hadronic responses. The upgraded MIPP spectrometer offers a unique opportunity to measure the neutral particle response to three neutral species, the neutron, the K_L^0 and the anti-neutron.

The basic idea is to use the diffractive reactions

$$pp \rightarrow n\pi^+p \quad (11)$$

$$K^+p \rightarrow \bar{K}^0\pi^+p; \bar{K}^0 \rightarrow K_L^0 \quad (12)$$

$$K^-p \rightarrow K^0\pi^-p; K^0 \rightarrow K_L^0 \quad (13)$$

$$\bar{p}p \rightarrow \bar{n}\pi^-p \quad (14)$$

where the beam of protons, K^\pm or \bar{p} fragments diffractively to produce the neutral beam. The charged particles in the reaction are measured in the MIPP spectrometer. The beam momentum is known to $\approx 2\%$. So the momentum of the tagged neutral particle can be

inferred by constrained fitting (3-C fit) to better than 2%, event by event. The tagged neutral particle goes along the beam direction and ends up in a test calorimeter placed in lieu of the present MIPP calorimeter.

This technique demands that the target is a proton and will only work on a liquid hydrogen cryogenic target (that MIPP possesses). The plastic ball recoil detector in the MIPP Upgrade will act as an additional veto against neutral target fragments such as slow π^0 's.

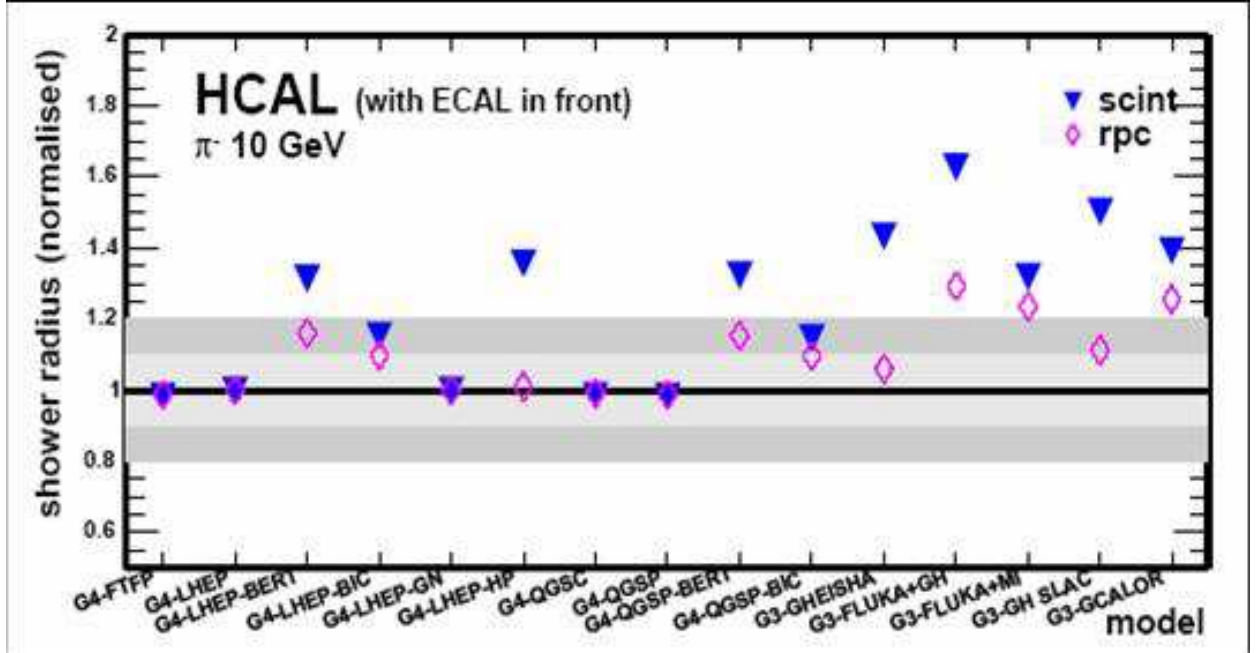


FIG. 15: The width of a 10 GeV/c π^- energy deposit in scintillator and RPC readout calorimeters as simulated by a host of simulation programs available in Geant4 (G4-) and Geant3 (G3-). The widths are normalized to the minimum width obtained.

The momentum spectrum of the neutral beam is controllable by changing the beam momentum. The method is outlined in detail in MIPP note 130 [21]. The diffractive processes are simulated using the program DPMJET and the event rates estimated for a calorimeter placed in the MIPP calorimeter position. With the MIPP upgrade, it should be typically possible to obtain $\approx 50,000$ tagged neutrons, $\approx 9,000$ tagged K_L^0 , and $\approx 11,000$ tagged \bar{n} per day in the calorimeter with the beam momentum set to 20 GeV/c. Table II shows the expected number of events /day as a function of beam momentum and beam species. Figure 16 shows the momentum spectrum of tagged neutrons accepted in the calorimeter as a function of the beam momentum. Other similar plots are available in

TABLE II: Expected number of tagged neutrons, K_L^0 , and anti-neutrons per day with an upgraded MIPP spectrometer.

Beam Momentum	Proton beam	K^+ beam	K^- beam	\bar{p} beam
GeV/c	n/day	K_L^0 /day	K_L^0 /day	\bar{n} /day
10	20532	4400	4425	6650
20	52581	9000	9400	11450
30	66511	12375	14175	13500
60	47069	15750	14125	13550
90	37600	-	-	

MIPP note 130 [21]. The acceptance of the calorimeter is assumed to be a circle of radius 75 cm about the beam axis, for the purposes of this calculation. The event is accepted only if a recoil proton of energy greater than 200 MeV is produced that is detected in either the plastic ball or the TPC. The rates quoted here are for an upgraded MIPP spectrometer operating at 3kHz DAQ rate, with a Main Injector spill of 4 sec duration delivered every 2 minutes and a beam downtime of 42%. These beam rates produce 12,000 interactions per spill (5 million interactions/day) which are recorded and stored on mass storage device. These events can be used for physics. The ILC calorimeter can be triggered using a “neutral energy deposited “ trigger and the calorimeter hits are read out only for those events. These events (maximum rates for inclusive neutrons are 3000 per spill) can be filtered and stored on a separate file in real time. The tagged neutral events can then be extracted using 3-Constraint kinematic fitting. The fitting will lead to an energy resolution event by event for each neutral particle entering the calorimeter of $\approx 2\%$.

G. Tagged π^0 's

The technique outlined here can also be used to produced tagged beam of π^0 's, which can be used to study the π^0 mass reconstruction capabilities of the ILC calorimeter. For

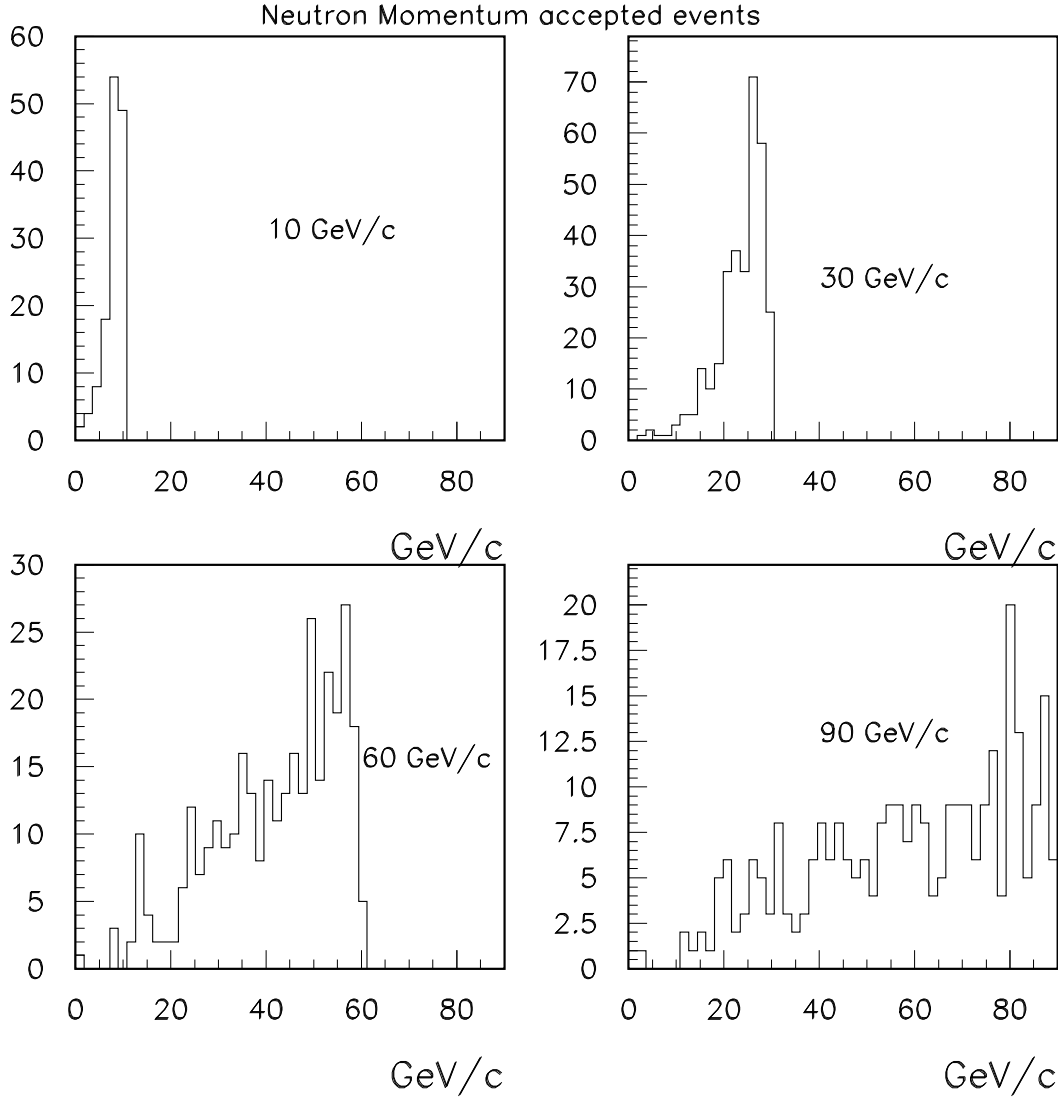


FIG. 16: Momentum spectrum of accepted neutrons for incident proton momenta of 10 GeV/c, 30 GeV/c, 60 GeV/c and 90 GeV/c for the process $pp \rightarrow pn\pi^+$.

this purpose, we employ beams of charged pions and employ the diffractive channels

$$\pi^+ p \rightarrow \pi^0 \pi^+ p \quad (15)$$

$$\pi^- p \rightarrow \pi^0 \pi^- p \quad (16)$$

$$(17)$$

The outgoing π^0 momentum can be solved using a 1-C fit, since we do not know the impact point of the π^0 . The mean momentum of the π^0 can be varied by changing the incoming beam momentum and in the cases where the π^0 decays in a fashion such that both photons end up in the calorimeter, one can solve for the energy of the two photons given their impact point in the calorimeter. One can also compare the calorimeter reconstructed π^0 mass to PDG values.

H. Simulation of jets in a test beam

So far we have only considered the problem of measuring the single particle response of calorimeters. An underlying assumption is that we can superpose single particle responses of particles to build the response to jets of particles. This assumes linearity of response and ignores problems such as coherent electronics noise etc.

Jets at the ILC consist of particles resulting in the fragmentation of all quark types (u,d,c,s,t,b). In the test beam, we only have access to particles made up of u, d, s quarks. Thus it is not feasible to reproduce the particle content and multiplicities of jets that will be encountered at the ILC in a test beam. One can however measure single particle response of the calorimeters to the six charged beam species π^\pm, K^\pm, p^\pm as well as the tagged neutral beams n, \bar{n}, K_L^0 and π^0 's. One can then use these single particle data to simulate the behavior of ILC jets assuming linear supersposition holds. Let us note that such studies will only describe the ILC jets in regions of phase space (dead material, angles of incidence) similar to the test beam calorimeter and will not in general simulate the effect of ILC tracking detector magnetic fields. However, this gives an idea of the behavior of jets in a full ILC detector.

Linear superposition is not guaranteed in calorimeters. Electronic cross-coupling (coherent noise) and saturation effects will in general work against such an assumption. So it may be desirable to study the response of the calorimeter prototype to multiple tracks hitting it simultaneously. This can be done by using the 5 million events/day written out at the tagged neutral beam. Events in which the beam particle dissociates diffractively contain forward going charged and neutral particles. The tagged neutral beam events form a subset of a much larger set of events in which forward going multiple particles exist. The MIPP spectrometer is so configured that the downstream magnet (ROSIE) bends the particles back in opposite direction to the Jolly Green Giant magnet in which the TPC sits. This results

in a large acceptance of particles above ≈ 7 GeV/c at the RICH detector and consequently the ILC calorimeter which will sit downstream of the detector. All these charged particles will be identified by the MIPP spectrometer and multiplicities of 4-5 at the RICH counter are quite common. So the 5 million events written out/day can be a rich source for studying multi-particle effects in the calorimeter. The momentum content of these particles can be varied by changing the MIPP primary beam momentum.

IV. CONCLUSIONS

We have outlined a two pronged approach to understanding the problem of understanding hadronic showers in calorimeters for the ILC. It entails obtaining new data to improve the shower simulation programs while simultaneously measuring the response to charged and tagged neutral beams to calorimeters.

We have outlined a scheme to construct a compensating highly segmented calorimeter cheaply that can be made compensating and also serve the interests of the PFA algorithm.

The program is ideal for training graduate students in the techniques employed in HEP. The impact of such a program will be beyond the ILC itself and will help cosmic ray energy systematics, atmospheric neutrino experiments and the ongoing worldwide neutrino oscillation program.

V. ACKNOWLEDGEMENTS

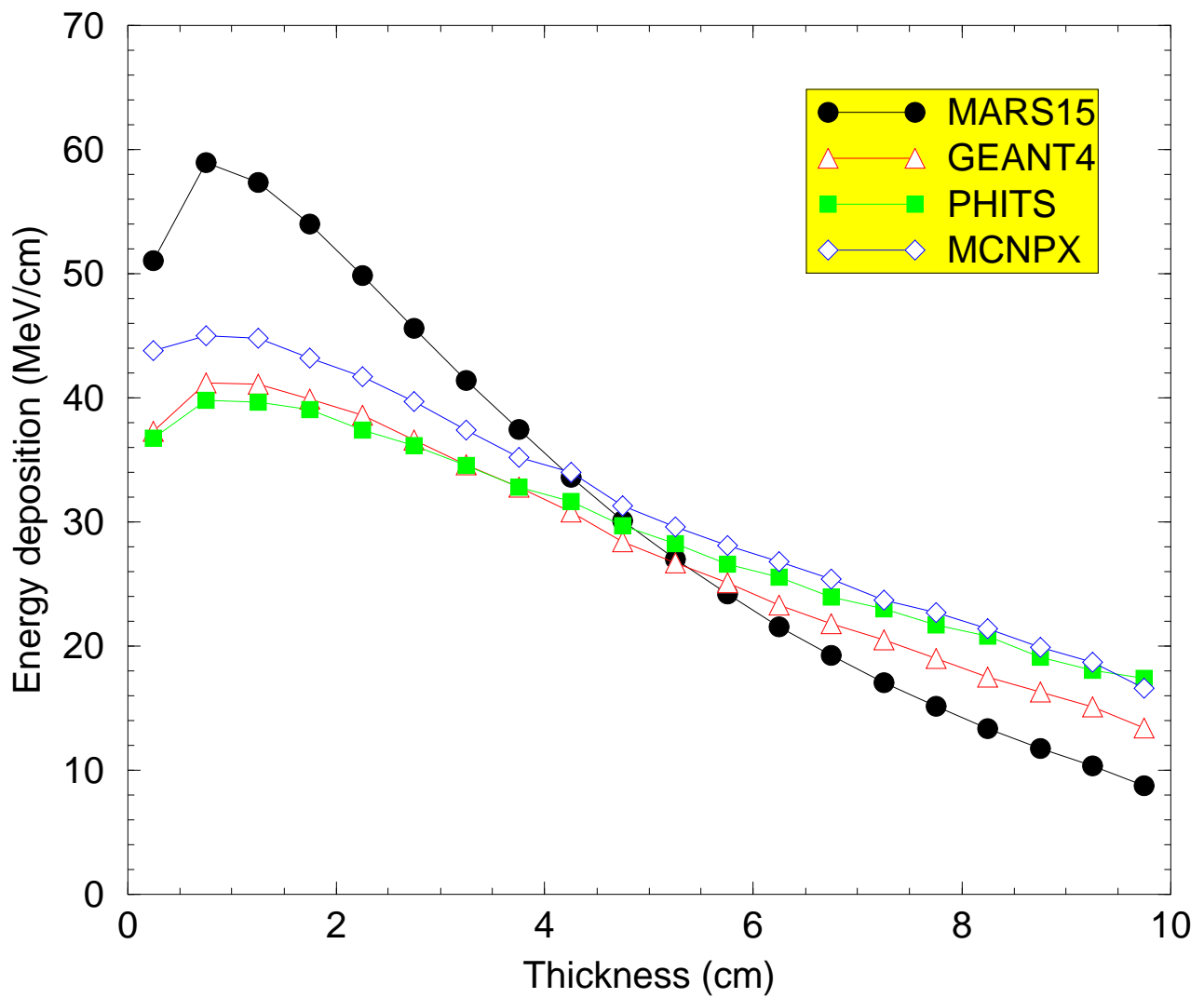
The author wishes to thank Robert Tschirhart for asking that such a paper as this be put together, Marcel Demarteau for general encouragement, Nikolai Mokhov and Sergei Strig-anov for providing the Monte Carlo validation plots and Stephen Pordes for conversations involving liquid argon TPC's. This work was supported by the U.S. Department of Energy.

[1] For the PFA concept, see for example, "Particle Flow Algorithm-Jets and Detector concepts", talk by J-C. Brient, LLR-Ecole Polytechnique at SNOWMASS 2005
www.slac.stanford.edu/econf/C0508141/proc/pres/ALCPG1106_TALK.PDF

- [2] The Hadronic Shower Simulator Workshop was held at Fermilab, September 6-8, 2006. Details may be found at <http://conferences.fnal.gov/hss06/> and proceedings have been published by AIP.
- [3] For details on DPMJET, please consult S Roesler, R. Engel, J. Ranft, hep-ph/0012252, Proc. of Monte carlo 2000, Lisbon, October 2000, Springer, p 033 (2000).
- [4] See for example G. Folger and J.-P. Wellisch, “String Parton Models in GEANT4”, CHEP03, La Jolla, California, March 2003, nucl-th/0306007.
- [5] A. Capella, U. Sukhatme, C. I. Tan, and J. Tran Than Van, Phys. Rep. **236**, 225 (1994).
- [6] See talk by Ralph Engel, “The Physics of the Models SIBYLL and DPMJET”, at the International Symposium on Very High Energy Cosmic Ray Interactions, 2006, Weihai, China, <http://isvhecri2006.ihep.ac.cn/isvhecri2006/index.py/home>
- [7] Fluka– A. Ferrari, P.R. Sala, A. Fassò and J. Ranft, CERN 2005-10 (2005), INFN/TC_05/11, SLAC-R-773;
Geant4 Collaboration –S. Agostinelli et al., Nucl. Instrum. Meth. **A506**, 250, (2003). J. Allison et al., IEEE Trans. Nucl. Sci. **53**, 270 (2006).
MARS– N.V. Mokhov, *Fermilab-FN-628* (1995); N.V. Mokhov et al, *Rad. Prot. Dosimetry*, **116**, 99 (2005); N.V. Mokhov et al, *Int. Conf. on Nucl. Data Sci. Technology, AIP Conf. Proc.*, PHITS–H. Iwase, K. Niita and T. Nakamura, *J.Nucl.Sci.Technol.* **39**, 1142(2002).
MCNPX–D. B. Pelowitz, ed., “MCNPX User’s Manual Version 2.5.0”, Los Alamos National Laboratory, LA-CP-05-0369(April 2005).
- [8] J. V. Allaby, F. Binon, A. N. Diddens, P. Duteil, A. Klovning and R. Meunier, “High-energy particle spectra from proton interactions at 19.2-GeV/c,”
- [9] K. N. Barish *et al.*, “Leading baryon production in p+A collisions at relativistic energies,” Phys. Rev. C **65**, 014904 (2002).
- [10] See “Hadronic Shower Intercomparison and Verification”, N. Mokhov and S. Striganov, in Proceedings of the Hadronic Shower Simulation Workshop, M. Albrow, R. Raja Editors, AIP.
- [11] See talk by Stefano Lami, “The Totem Experiment at the LHC”, at the International Symposium on Very High Energy Cosmic Ray Interactions, 2006, Weihai, China, <http://isvhecri2006.ihep.ac.cn/isvhecri2006/index.py/home>
- [12] Information on the MIPP Experiment can be found at <http://ppd.fnal.gov/experiments/e907/>
- [13] The MIPP upgrade proposal can be found at

- <http://ppd.fnal.gov/experiments/e907/notes/MIPPnotes/public/pdf/MIPP0138/MIPP0138.pdf>
- [14] See Calorimeter-Energy Measurement in Particle Physics. R Wigmans, Oxford Science Publications, Page 71.
 - [15] “CMS Validation Experience: testbeam 2004 data vs. Geant4”, S. Piperov, in Proceedings of the Hadronic Shower Simulation Workshop, M. Albrow, R. Raja Editors, AIP.
 - [16] “On sampling fractions and electron shower shapes”, A. Peryshkin and R. Raja, DØ Note 1215
<http://ppd.fnal.gov/experiments/e907/notes/MIPPnotes/public/pdf/MIPP0036/MIPP0036.pdf>
 - [17] “Hadron and jet detection with a dual-readout calorimeter”, N. Akchurin et. al, NIMA, Volume **537**, Issue 3, (2005) P.537.
 - [18] Kirk. T. McDonald, “Large and Small (Far and Near) Liquid Argon Detectors for an Off-Axis NuMi beam”, talk given at the NuMi Off-Axis Experiment Detector Workshop, SLAC, Jan 23-24, 2003.
<http://puhep1.princeton.edu/~mcdonald/nufact/>
 - [19] Documentation on the ILC detector concepts can be accessed from
<http://physics.uoregon.edu/~lc/wwstudy/concepts/> More information on ILC detector groups can be found at
 SiD—<http://www-sid.slac.stanford.edu/>
 LDC—<http://www.ilcldc.org/>
 GLD—<http://ilcphys.kek.jp/gld/>
 DREAM—This is the 4th concept of a detector and is centered around the compensating calorimeter using dual-readout fibers [17]
 - [20] G. Mavromanolakis, U. of Cambridge/Fermilab, Private Communication.
 - [21] “Tagged Neutron, Anti-neutron and K_L^0 beams in an Upgraded MIPP Spectrometer”, R. Raja, MIPP Note 130,
<http://ppd.fnal.gov/experiments/e907/notes/MIPPnotes/public/pdf/MIPP0130/MIPP0130.pdf>

1-GeV proton on 10-cm tungsten rod (R=1 cm)



50-GeV proton on 10-cm tungsten rod (R=1 cm)

